The x-ray light valve: A potentially low-cost, digital radiographic imaging system—a liquid crystal cell design for chest radiography

Timothy C. Szeto, Christie Ann Webster, Ivaylo Koprinarov, and J. A. Rowlands[a)]
Imaging Research, University of Toronto, Sunnybrook Health Sciences Centre, 2075 Bayview Avenue, Toronto, Ontario, M4N 3M5, Canada

(Received 27 June 2007; revised 5 January 2008; accepted for publication 8 January 2008; published 20 February 2008)

Digital x-ray radiographic systems are desirable as they offer high quality images which can be processed, transferred, and stored without secondary steps. However, current clinical systems are extraordinarily expensive in comparison to film-based systems. Thus, there is a need for an economical digital imaging system for general radiology. The x-ray light valve (XLV) is a novel digital x-ray detector concept with the potential for high image quality and low cost. The XLV is comprised of a photoconductive detector layer and liquid crystal (LC) cell physically coupled in a sandwich structure. Upon exposure to x rays, charge is collected at the surface of the photoconductor, causing a change in the reflective properties of the LC cell. The visible image so formed can subsequently be digitized with an optical scanner. By choosing the properties of the LC cell in combination with the appropriate photoconductor thickness and bias potentials, the XLV can be optimized for various diagnostic imaging tasks. Specifically for chest radiography, we identified three potentially practical reflective cell designs by selecting from those commonly used in LC display technology. The relationship between reflectance and x-ray exposure (i.e., the characteristic curve) was determined for all three cells using a theoretical model. The results indicate that the reflective electrically controlled birefringence (r-ECB) cell is the preferred choice for chest radiography, provided that the characteristic curve can be shifted towards lower exposures. The feasibility of the shift of the characteristic curve is shown experimentally. The experimental results thus demonstrate that an XLV based on the r-ECB cell design exhibits a characteristic curve suitable for chest radiography.
[DOI: 10.1118/1.2839105]

I. INTRODUCTION

The most advanced digital radiographic imaging system in clinical use, the active matrix flat panel imager (AMFPI), is a self-scanned detector which utilizes thin-film-transistor arrays to store and, at the appropriate time, transfer image data off the detector for digitization and display.[1] Although AMFPIs have high image quality, they are expensive to manufacture. As an alternative, Rieppo and Rowlands[2] proposed a novel x-ray image detector, the x-ray light valve (XLV), which incorporates several stages (x-ray absorption, image formation, and amplification) within a simple, compact structure and eliminates the problems caused by a secondary quantum sink. Theoretical evaluations demonstrated that an XLV using amorphous selenium (*a*-Se) is feasible for clinical radiographic applications.[3,4] Recently, Rowlands *et al.*[4,5] proposed modifying the initial concept by replacing the charge coupled device camera with an optical scanner and utilizing a reflective approach for image readout. These improvements allow the system to be scaled to the number of pixels as required by the application and simplify the optics of the readout system.

An overview of the structure and operation of the XLV is shown in Fig. 1. A more detailed description can be found elsewhere.[4] The XLV consists of an *a*-Se layer and liquid crystal (LC) cell physically and electrostatically coupled in a sandwich structure [see Fig. 1(a)]. A large potential, V_E, is applied to the electrodes to create an electric field across the photoconductor during the exposure step of operation. Upon x-ray irradiation, electron-hole pairs are formed within the *a*-Se layer. The presence of the electric field immediately separates the charges, which drift towards opposite surfaces of the photoconductor [see Fig. 1(b)]. After the exposure is completed, V_E is reduced to a smaller potential, V_R. The charge collected at the *a*-Se-LC interface creates an image electric field that correspondingly causes a change in the reflective properties of the LC cell. A visible image is thus formed and digitized by an optical scanner during the readout stage of operation [see Fig. 1(c)]. By choosing the appropriate design parameters of the LC cell, thickness of the *a*-Se layer, and operating parameters such as V_R and V_E, the XLV can be optimized for various imaging tasks. Any one of several LC designs could potentially be used in the XLV, including the electrically controlled birefringence (ECB) cell, twisted nematic (TN) cell, and polymer dispersed liquid crystal (PDLC) cell.[4,6] The purpose of this article is to assess a range of different designs and determine which is most appropriate for clinical chest radiography.

II. XLV DESIGN REQUIREMENTS

In order to be clinically useful, novel digital detectors must surpass or at least match the performance of conventional benchmarks. Zhao and Rowlands[7] identified imaging

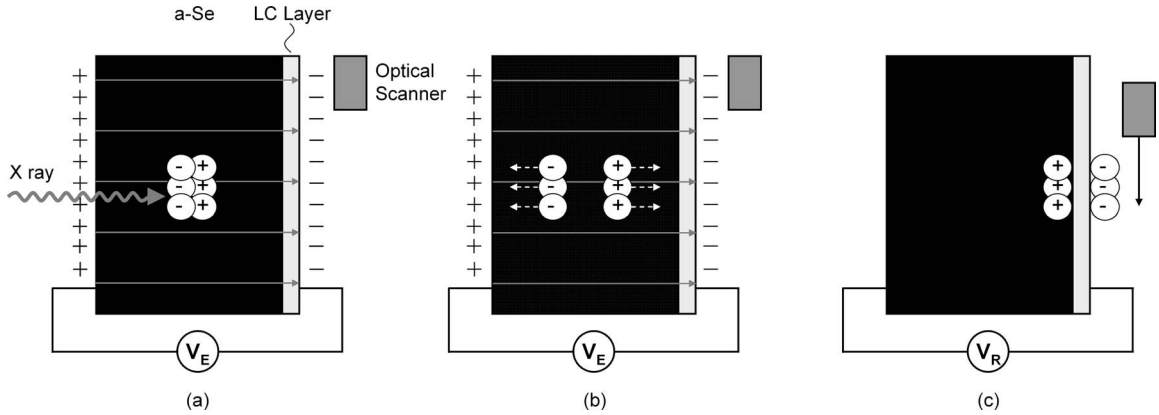

FIG. 1. Basic structure and operation of the x-ray light valve. (a) X rays are absorbed in the photoconductive *a*-Se layer, generating electron-hole pairs within a localized region. (b) A large electric potential (V_E) guides the electrons and holes to opposite surfaces of the photoconductor. Once exposure is completed and V_E is removed, the electric field created by the charges trapped at the *a*-Se-LC interface induces a visible image in the LC cell. (c) An optical scanner digitizes the visible image while a small electric potential (V_R) is applied.

requirements for digital radiographic detectors. In particular, the requirements and specifications for chest radiography are shown in Table I.

An imaging system based on the XLV concept can readily satisfy the size requirement for chest radiography of 35 $\times$43 cm (or even 45$\times$45 cm favored by some manufacturers) without increased complexity. Large area *a*-Se detectors are feasible and cost effective because the photoconductor is amorphous and can be made through evaporation techniques on relatively cool ($\sim$50 °C) substrates.[8] LC technology is well established within the display industry and cells can be made large enough to meet the size requirement. Furthermore, the scanning approach permits the device to be scalable without sacrificing resolution or total number of pixels.[4]

The requirement for pixel size and the corresponding resolution can also be fulfilled since *a*-Se is an electrostatic detector in which little blurring occurs.[9] The presence of the electric field during exposure to x rays ensures that there is minimal lateral spread in the image charge. Thus, the charge collected at the *a*-Se-LC interface accurately reproduces the absorbed x-ray intensity pattern, even for a thick *a*-Se layer. Furthermore, LC cells inherently have a resolution on the order of a few microns and will not be the limiting factor.[4] Considering that available optical scanners also have ample resolution and pixel count, an adequate image resolution can be achieved with a photoconductor layer thick enough to provide high quantum efficiency at a 120 kVp spectrum.[4]

TABLE I. Design requirements of digital x-ray detectors for chest radiography.

Design requirement	Specification
Detector size (cm)	35$\times$43
Pixel size (μm)	200$\times$200
Number of pixels	1750$\times$2150
Image readout time (s)	$<$5
X-ray spectrum (kVp)	120
Mean exposure to image	0.3
detector (mR)	0.3
Exposure range (mR)	0.03–3

The readout time of the XLV is governed by the mechanics and electronics of the optical scanner, both of which can be adjusted to reduce the scan time to less than 5 s. Nonetheless, the most important requirement for an x-ray detector is its overall response to x rays, also known as the characteristic curve. In the case of the XLV, the response within the exposure range of 0.03–3 mR (7.74–774 nC/kg) will strongly depend on the characteristic response curve of the LC cell.[4] To evaluate different LC cell designs which are able to fulfill this requirement, it is necessary to determine the optical response of each cell as a function of the amount of image charge collected on the surface of the photoconductor, which in turn is proportional to the amount of x-ray exposure.

In addition to the medical requirements listed in Table I, further design considerations related to the construction of the XLV must be taken into account. To minimize the effects of x-ray quantum noise at low exposures and to achieve a reasonable signal-to-noise ratio throughout the exposure range, it would be desirable to use a LC cell design which is dark in the nonexposed state and bright in the exposed state. In addition, the ideal LC cell should have a time constant long enough to be able to retain an image charge at the *a*-Se-LC interface during image scanning.[4] Additional concerns are the reliability, lifetime, and ease of manufacturability of the LC cell.

III. REFLECTIVE XLV DESIGNS

In the construction of an XLV, two main components may be adjusted to modify the characteristic response to x-ray exposure: the electro-optical properties of the LC cell and the thickness of the photoconductive *a*-Se layer.

III.A. Liquid crystal cell

When designing a LC cell, numerous choices can be made, including the initial orientation of the LC molecules,

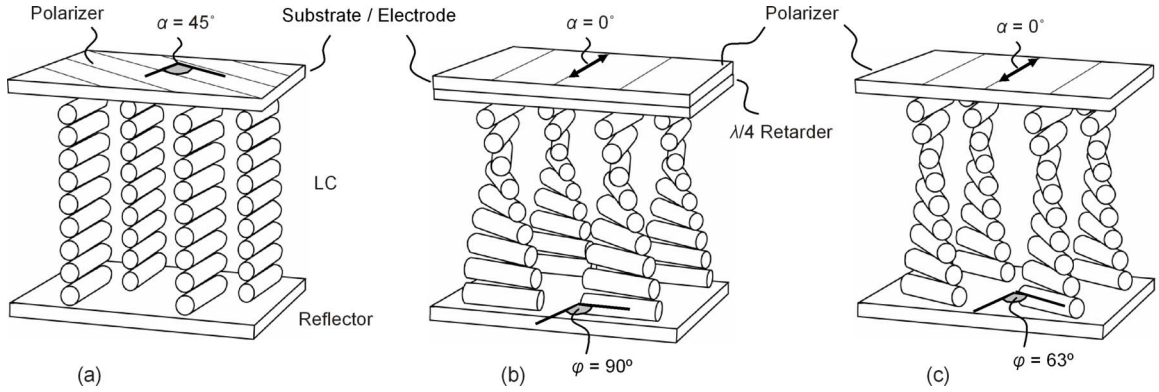

FIG. 2. Optical arrangements for the three reflective liquid crystal cell designs of interest, consisting of a polarizer oriented at an angle α to the director of the uppermost nematic LC molecules, a LC layer twisted by an angle φ, and a reflective surface (reflector) at the base. The diagrams shown are (a) r-ECB cell with α=45° and φ=0°, (b) 90° r−TN cell with α=0° and φ=90°, and (c) 63° r−TN cell with α=0° and φ=63°. A quarter-wave retardation plate oriented 45° azimuthally to the director is used within the optical stack of the 90° r−TN cell.

angle of the polarizer and analyzer, degree of twist of the LC molecules from top to bottom of the cell, thickness of the cell, and properties of the LC mixture.[4] Each combination produces its own electro-optical response. Focusing on the technically preferable reflective approach,[4] we identified three promising cells: reflective ECB (r-ECB), 90° reflective TN (90° r−TN), and 63° reflective TN (63° r−TN). The PDLC cell was not included in this list since it was reported to have a time constant of about 5 s[6] and thus may show image fading during the digitization of the optical image.

Figure 2 illustrates the three designs of interest. The orientation of the LC molecules in TN cells is described by the *director*,[4] which points in the preferred direction of the LC molecules at any point within the cell. The azimuthal angle between the topmost director and bottommost director is termed the *twist angle*, φ.[4] Each of the proposed cells share the same basic structure, consisting of a polarizer oriented at an azimuthal angle of α with respect to the uppermost director, a nematic LC layer with a twist of φ, and a reflector (or a reflective surface) at the bottom. Before applying an electric field, the director of the LC molecules is parallel to the surface of the LC layer and the electrodes of the cell (see Fig. 2). When a potential is applied to the electrodes, the electric field causes the LC molecules to tilt in the direction of the field lines and the original arrangement is eliminated.[4] However, it should be noted that there is a minimum voltage or *threshold voltage*, V_{th}, required to overcome the elastic torque before any reorientation occurs.[4,10]

The r-ECB cell [see Fig. 2(a)] has α=45° and φ=0°.[4,11] The cell acts as a variably birefringent sheet where the retardation can be controlled by an applied electric field. The cell thickness, d_{ECB}, is usually chosen such that, when no potential is applied, the phase difference is exactly one half of a cycle (also known as *half-wave retardance*).[4] For a reflective cell, this is attained when the following relationship is satisfied:[4,11]

$$d_{ECB} = \frac{\lambda}{4\Delta n}, \tag{1}$$

where λ is the wavelength of the incident light and Δn is the birefringence of the LC molecules. It should be noted that if r-ECB cells are made thicker (i.e., $d > d_{\text{ECB}}$), the characteristic electro-optical response becomes multi-valued. Nonetheless, the ratio of the brightest state to the darkest state remains constant, resulting in no loss of total available contrast.

As the name implies, the 90° r−TN cell [see Fig. 2(b)] has α=0° and a twist angle φ=90°.[4,11] To obtain the same effect as the crossed-polarizer configuration, the polarizer is followed by a $\lambda/4$ wave plate oriented 45° azimuthally to the polarizer.[4] The optimum thickness of the 90° r−TN cell can be obtained from the Gooch and Tarry formula,[12] derived for a transmissive 90° TN (90° t−TN) cell. In the case of a reflective cell, the light propagates twice through the LC layer, which means that the reflective configuration requires only half of the thickness as compared to its transmissive counterpart.[4] For a 90° t−TN cell, the light transmission is described by[3,12]

$$T = \frac{1}{1+u^2}\sin^2\varphi\sqrt{1+u^2}, \tag{2}$$

$$u \doteq 2d_{90°t-TN}\frac{\Delta n}{\lambda}, \tag{3}$$

where u is defined to be the normalized retardation parameter and $d_{90°\text{t−TN}}$ is its thickness. The maximum contrast ratio occurs at the minima where T=0 in Eq. (2), at the specific values of $u=\sqrt{3}, \sqrt{15}, \sqrt{35}\ldots$

The 63° r−TN cell [see Fig. 2(c)] has α=0° and φ=63.64°.[13] The thickness and twist angle of the cell are chosen such that linearly polarized input light is circularly polarized upon arrival at the reflector. The handedness of circular polarization switches upon reflection and the light

leaving the cell has linear polarization rotated 90° from the direction at the input. This effect only occurs when both of the following equations are satisfied:[14]

$$\varphi = \frac{(2N-1)\pi}{2\sqrt{2}}, \tag{4}$$

$$d_{63°r-TN}\Delta n = \frac{(2N-1)\lambda}{2\sqrt{2}}, \tag{5}$$

where $N=1,2,3,\ldots$. The first two solutions ($N=1,2$) from these two equations are $(\varphi, d_{63°\text{r-TN}}\Delta n)=(63.64°, 0.354\lambda)$ and $(190.9°, 1.061\lambda)$. The first result is more desirable since it gives better performance in terms of contrast, thus giving rise to the 63° r−TN cell.

III.B. Photoconductive *a*-Se layer

The thickness of the photoconductive *a*-Se layer plays a critical role in determining the amount of charge collected at the *a*-Se-LC interface following x-ray exposure. For a quantum-efficient system, it is necessary to have an *a*-Se layer thick enough to absorb as many x rays as possible. Assuming an exposure, X, of monoenergetic x rays and no bulk trapping of x-ray generated charge, the image charge, Q, at the interface can be calculated by using the relationship[3,4]

$$Q = XN_R\eta(\xi/W_{\pm})e, \tag{6}$$

where N_R is the number of photons per unit area per Roentgen, η is the x-ray quantum efficiency of the *a*-Se layer, ξ is the x-ray energy, $\xi/W_{\pm}$ is the quantum gain or the number of electron-hole pairs released per x-ray photon, and e is the elementary charge of an electron. It has been shown experimentally that the $W_{\pm}$ of *a*-Se is a function of electric field, E, with the following dependency:[15]

$$W_{\pm} = 50\left(\frac{E}{10}\right)^{\alpha}, \tag{7}$$

where α is ~−0.8 and at a typical bias electric field E of 10 V/μm, $W_{\pm}$ is ~50 eV.[16] Taking into account the voltage-dependent capacitance $C(V)$ of the LC layer,[17] the signal potential V which results across the LC cell can then be derived as a function of X using Eq. (6) and the relationship

$$Q = \int_0^V C(V)dV. \tag{8}$$

IV. MODELING THE CHARACTERISTIC CURVES OF DIFFERENT XLV DESIGNS

A theoretical model was used as an initial evaluation to determine which of the three LC cell designs has the best potential to fulfill the requirements for chest radiography. The model enabled the prediction of the optical responses of the cells as a function of V, which were subsequently converted into functions of Q, and ultimately as functions of X.

Modeling of the three designs of interest was performed with GNU-LCM,[18] a LC simulation program developed at Kent State University. In a companion paper,[17] it was shown that GNU-LCM gives satisfactory results in predicting the characteristic curve of an XLV, while also considering the voltage-dependent capacitance of the LC layer. Since all three cells operated in a reflective mode, the Berreman 4 ×4 matrix method[19] was used to account for multiple reflections and oblique incident light. A summary of the modeling parameters of each individual layer within the three different cell structures is given in Table II. With the exception of the cell-specific parameters (i.e., cell thickness, polarizer orientation, and twist angle), all other parameters were based on the ZLI 4792 LC mixture[20] and on the availability of components. The appropriate cell thicknesses were determined for $\lambda=655$ nm, which is the peak wavelength of the light-emitting diode (LED) readout light used in our optical scanners. By applying Eq. (3) for the 90° r−TN cell, and Eq. (5) for the 63° r−TN cell, the thicknesses of the LC layers were calculated to be 2.39 and 2.83 μm, respectively. Equation (1) indicates that the thickness of the r-ECB cell should be 1.69 μm. However, cells that are this thin are too difficult to make reliably. Since there is no loss of total available contrast with a thicker cell, a thickness of 3.8 μm was chosen for the r-ECB cell based on the availability of spacers of this size. The problem of a multi-valued optical response for cells thicker than 1.69 μm can later be eliminated by modifying the bias potential during the digitization step in order to shift the curve towards lower exposures.[4] The viewing angle was chosen to be 20°, which is determined by the geometry of our optical scanners.

Given the input parameters, the modeling program was used to determine the physical orientation of the LC molecules within a specified range of externally applied potentials, V. In doing so, the relationships of reflectance versus potential and capacitance versus potential were established.[17] By using the information from both curves in combination

TABLE II. Modeling parameters for three different LC cell designs.

Parameter	r-ECB	90° r−TN	63° r−TN
Polarizer			
Active thickness (μm)	3	3	3
Azimuthal angle α (deg)	45	0	0
Glass			
Refractive index	1.52	1.52	1.52
Thickness (μm)	500	500	500
ITO			
Refractive index	1.81	1.81	1.81
Thickness (μm)	225	225	225
Alignment layer			
Refractive index	1.52	1.52	1.52
Thickness (μm)	0.5	0.5	0.5
Retarder			
Thickness (μm)	N/A	1.60	N/A
LC			
Twist angle φ (deg)	0	90	63.64
Thickness (μm)	3.80	2.83	2.39
Birefringence Δn	0.0968	0.968	0.968
Dielectric anisotropy ($\Delta\varepsilon$)	5.3	5.3	5.3

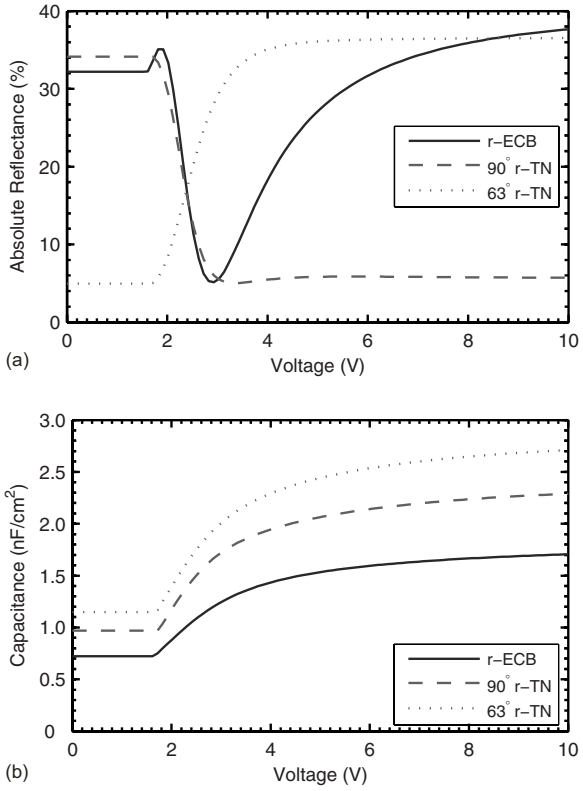

FIG. 3. Theoretical curves for the three reflective LC cell designs of interest, illustrating (a) reflectance vs applied potential and (b) capacitance vs applied potential. The parameters of the optical stacks used in the cells are summarized in Table II.

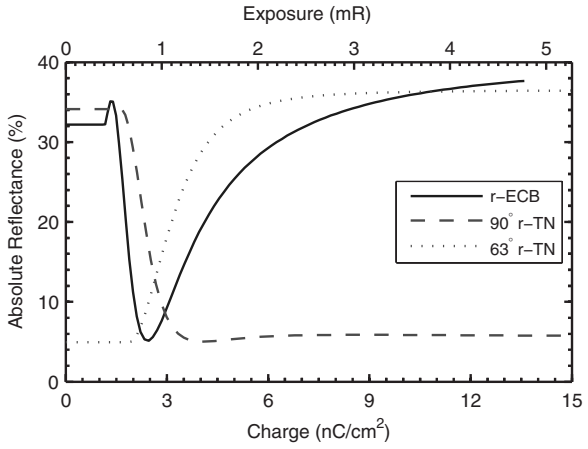

FIG. 4. Theoretical curves of the three reflective LC cell designs of interest, showing absolute reflectance as a function of charge (bottom axis) and exposure (top axis). The conversion between charge and exposure is based on a 1-mm-thick *a*-Se layer, an x-ray spectrum of 120 kVp, 4.1 mm of added aluminum filtration, and an operating distance of 1.65 m.

with Eq. (8), the reflectance was obtained as a function of charge Q. The charge axis was then converted into an equivalent x-ray exposure X by using Eqs. (6) and (7). This conversion was based on a 1-mm-thick *a*-Se layer, an x-ray spectrum of 120 kVp, 4.1 mm of added aluminum filtration, and an operating distance of 1.65 m. Hence, the calculated results were $\xi=57.6$ keV, $N_R=2.41\times10^8$ photons mm^{-2} R^{-1}, and $\eta=70.4\%$.[21]

In Fig. 3(a), the reflectance values of each cell, expressed as a percentage of intensity of the input light, are plotted as a function of V. Characteristic for all three cells is a V_{th} of ~1.6 V, which must be exceeded before any change in optical activity is observed. As expected, the optical response of the r-ECB cell is multi valued due to a cell thickness greater than 1.69 μm. Nonetheless, the absolute contrast is still comparable to the absolute contrasts of the other two cells. The r-ECB cell is optically active in a range between 1.6 and 10 V, marked by an initial steep descent, followed by a gradual increase in reflectivity. The optical response of the 90° r−TN cell decreases monotonically in a much narrower range of 1.6–3 V. Similarly, the 63° r−TN cell is also characterized by a fairly narrow range of optical response, increasing monotonically between 1.6 and 4 V. In Fig. 3(b), all three cells exhibit a voltage-dependent capacitance after V_{th} is surpassed, due to the dielectric anisotropy of the LC molecules. Dissimilarities in $C(V)$ can be explained by the different thickness of the three cells.

Figure 4 illustrates the absolute reflectance of all three cells as a function of Q (bottom axis) and X (top axis). The r-ECB cell reveals an optical response for exposures in the range of 0.5–4.5 mR (0.13–1.2 μC/kg), while both TN cells are only active in the relatively narrow ranges of 0.6–1.2 mR (0.15–0.31 μC/kg) and 0.7–2 mR (0.18–0.51 μC/kg) respectively. Because of the threshold voltage, none of the three cells can be used directly for imaging at low x-ray exposures. However, as proposed in Ref. 4, the curves can be shifted to the left (i.e., towards lower exposures) by applying a readout bias potential, V_R, during the digitization step, effectively permitting operation at low exposure levels for all three cells.

Nonetheless, only the r-ECB cell has an operational range spanning the full exposure range of 0.03–3 mR (7.74–774 nC/kg), as required for chest radiography (see Table I). In addition, if a sufficient V_R is applied, the curve of the r-ECB cell will be shifted far enough to the left to have a monotonically increasing response. Thus, among the three cells which have been analyzed theoretically, the r-ECB has the greatest potential to fulfill all the requirements for chest radiography, provided that the characteristic curve can indeed be shifted towards lower exposures. Later in this article, we will demonstrate experimentally that such a shift is practically feasible.

V. METHODS AND MATERIALS

An XLV prototype employing an r-ECB cell design was constructed using a mixture of ZLI 4792 LC molecules with a birefringence of $\Delta n=0.0968$ [see Fig. 5(a)]. The LC layer was sandwiched between a 150-μm-thick *a*-Se layer and transparent indium tin oxide (ITO) layer evaporated onto a 0.5-mm-thick glass substrate. To provide rigidity, the *a*-Se was evaporated onto a 2.1-mm-thick aluminum substrate. A detailed description of the construction process can be found elsewhere.[4] Together, the ITO and aluminum substrate act as

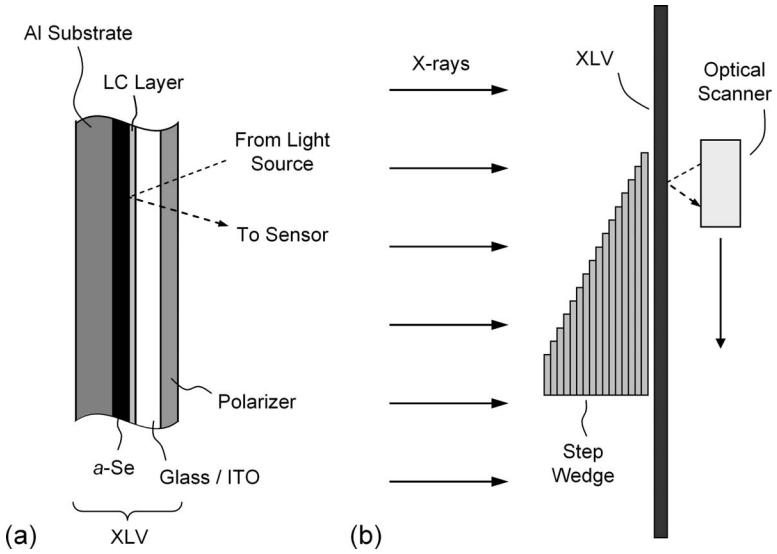

FIG. 5. XLV structure and experimental setup used for measuring the effect of a readout bias potential applied during the digitization step of XLV operation. In (a), the layers comprising the XLV are shown. In (b), a step wedge is placed against the XLV to obtain the characteristic curve. During exposure, a 10 V/μm electric field is maintained across the XLV. Following exposure, the electric field is lowered or completely turned off while the induced image in the LC cell is digitized with an optical scanner.

the electrodes for the application of the bias potentials. The thickness of the cell was chosen to be 3.8 μm, based on the availability of spacers of this size. The properties of the optical components used to make the XLV prototype are listed in Table II.

For digitization of the optical image, a commercial paper scanner (CanoScan LiDE 30, Canon Inc.) was used, the head of which was modified to accommodate the specularly reflective geometry as described elsewhere,[4] producing a 40° angle between incident and reflected light [see Fig. 5(a)]. Using in-house software, the scanner was operated in 8 bit mode in its full native resolution of 1200 dpi (dots per inch) after standard calibration was applied. The illumination of the scanner consisted of three identical red LEDs having a peak emittance at 655 nm.

Figure 5(b) illustrates the experimental apparatus used to measure the reflectance of the XLV prototype. The XLV was placed 1.65 m away from the x-ray tube, operated at 60 kVp and 2.0 mm of added Al filtration. The low energy x-ray beam was chosen because of the relatively thin layer of *a*-Se used in our prototype. During the exposure phase, V_E was set to 1500 V, which corresponds to an electric field of 10 V/μm in the *a*-Se layer. After the x-ray exposure, the bias potential was dropped to V_R for the digitization step. The timing sequence of the XLV operation is illustrated in Fig. 6. A 2 MΩ resistor connected in parallel with the high voltage power supply ensured that the bias changed rapidly between V_E and V_R. After each exposure, the XLV was rested for 48 h with the electrodes shorted to ensure that all trapped charges were completely removed from the photoconductor and that the experiments were reproducible. This procedure was used as a standard. Although rapid erasure in a time frame of 1–2 min is possible with appropriate light sequences, as employed by the flat-panel detector with trapped charges at the interface of an insulating layer,[22] this method requires further investigation.

Regions of different x-ray exposures were created in a single image by using a step wedge [see Fig. 5(b)]. The step wedge consisted of 16 aluminum plates stacked together, each with a thickness of 1.61 mm. A 5-mm-thick lead piece was placed in the field of view as a zero exposure reference. The data points for the different exposures were obtained by averaging areas corresponding to a minimum of 125 000 pixels. The relative reflectance was calculated by dividing the averaged grayscale values by the maximum 8 bit value (255) and rescaling to 100%. Images of the step wedge were acquired at various V_R. In order to measure the exposure behind each step, the aluminum plates were separated and the XLV system was replaced by an ionization chamber (Inovision, Model 35040). An additional

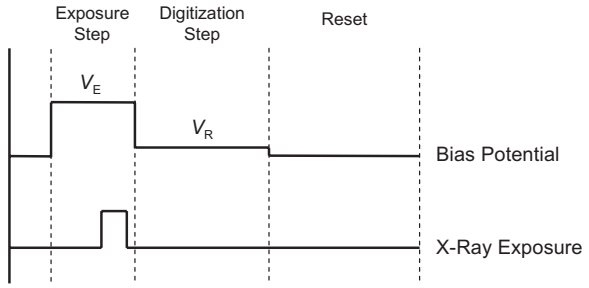

FIG. 6. Timing diagram of the operation of the XLV. During the exposure step, an exposure bias potential V_E is set to 1500 V, which corresponds to ~10 V/μm across the *a*-Se layer. Following x-ray exposure, V_E is reduced to a readout bias potential V_R for the digitization step. Subsequently, the bias potential is removed and the image charge is erased during the reset phase.

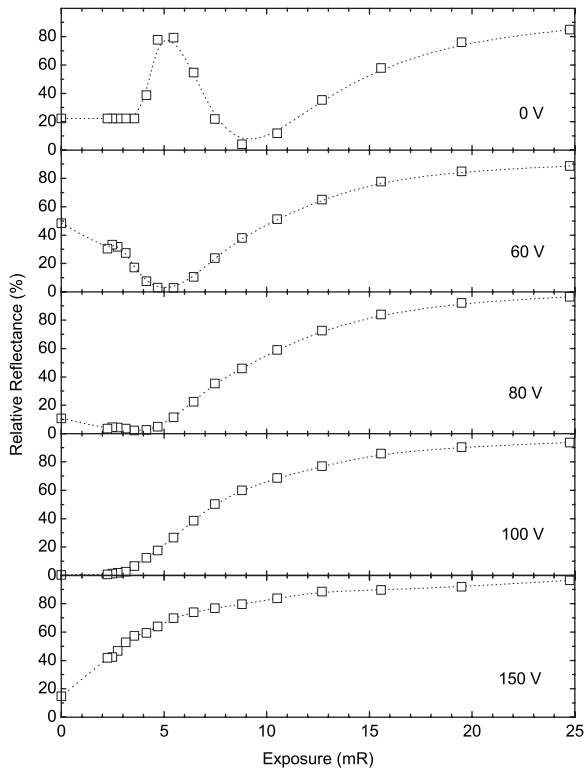

FIG. 7. Effects of various readout bias potentials on the measured characteristic curve of the XLV prototype. As increasing potential is applied, the curve shifts towards lower exposures. At 100 and 150 V, the curve is shifted significantly enough such that the originally multi-valued optical response becomes monotonically increasing. The data points were extracted from the grayscale values of a step wedge imaged with V_E=1500 V (~10 V/μm). In the second pane, the numbers beside each data point indicate the step number (0 stands for no step). Since a large number of pixels were averaged together, the standard error is too small to be shown.

2.1-mm-thick Al plate was placed in front of the chamber to account for the substrate on which the *a*-Se was evaporated [see Fig. 5(a)]. As plates were added in front of the chamber one by one, the exposure behind the corresponding number of plates was measured.

VI. RESULTS AND DISCUSSION

Figure 7 illustrates the effect of the readout bias potential V_R in the range of 0–150 V on the characteristic curve of the XLV prototype. The curve obtained for V_R=0 V is in good agreement with the theoretical curve derived for the r-ECB cell [see Fig. 3(a)]. The small differences may be attributed to the structural defects in the XLV prototype. As predicted in Ref. 4, the characteristic curve of the XLV shifts towards lower exposures with increasing V_R. It is evident that at V_R =100 and 150 V, the curve is shifted enough that the originally multi-valued optical response becomes monotonically increasing.

Our experimental prototype consisted of a relatively thin *a*-Se layer (150 μm) and a 60 kVp x-ray spectrum was used to match this thickness. However, a device designed for chest radiography should consist of a 1-mm-thick *a*-Se layer for sufficient quantum efficiency, which is also the thickness

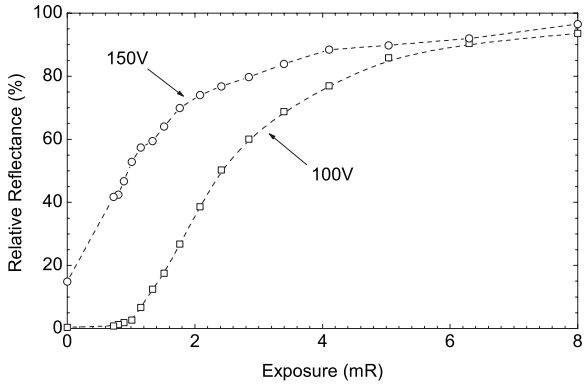

FIG. 8. Characteristic curves of the XLV prototype acquired with 100 and 150 V readout bias potential, rescaled for 1 mm *a*-Se thickness and 120 kVp x-ray spectrum.

used in some AMFPIs.[1] Hence, to properly evaluate the r-ECB cell design, we rescaled the experimental data on the basis of the expected change in x-ray-to-charge conversion. By using a 1-mm-thick *a*-Se layer and 120 kVp x-ray spectrum [see Table I], η increases from 43.9% to 70.4%, N_R increases from 1.83×10^8 to 2.41×10^8 photons/mm^2, and ξ increases from 39.4 to 57.6 keV.[21] Altogether, the exposure axis of Fig. 7 is scaled by a factor of 0.3233, resulting in Fig. 8. It is then evident that the characteristic curve acquired with V_R=150 V spans the full 0.03–3 mR (7.74–774 nC/kg) exposure range at energies used for chest radiography. It must be noted that the optimal V_R depends linearly on the thickness of the XLV which, in turn, is determined by the thickness of the *a*-Se layer. For a thinner XLV, a smaller readout bias potential would be adequate to shift the characteristic curve.

To demonstrate the curve shift due to a V_R, Figs. 9(a) and 9(b) show a 0.05-mm-thick lead star phantom acquired on our XLV prototype with V_R=0 and 40 V, respectively. It can be seen that the top image is the negative of the bottom image. For these images, the x-ray tube was operated at 60 kVp and 20 mAs, resulting in an exposure of 11.35 mR (2.92 μC/kg) at the detector and 4.4 mR (1.14 μC/kg) beneath the lead. The reason for the drastic change in the appearance of the images is that, in the case of V_R=0 V, the section of the characteristic curve with negative slope [see Fig. 7] is used, while in the case of V_R=40 V, the positive slope is used. In Fig. 9(a), the areas covered by the lead received a small amount of exposure, enough to bias the LC molecules into the brightest region of the characteristic curve (i.e., near the local maximum). In the areas where no lead was present, there was enough exposure to reach the dark region of the curve (i.e., near the local minimum). However, in Fig. 9(b), a potential of V_R=40 V shifted the characteristic curve towards lower exposures, causing the same x-ray exposure to lie on the positively sloped section of the curve. This effectively inverts the grayscale in the image so that areas with low exposure appear dark and areas with higher exposure appear bright. Both images show high contrast. It is apparent from the 15 times magnified inset images, Fig. 9

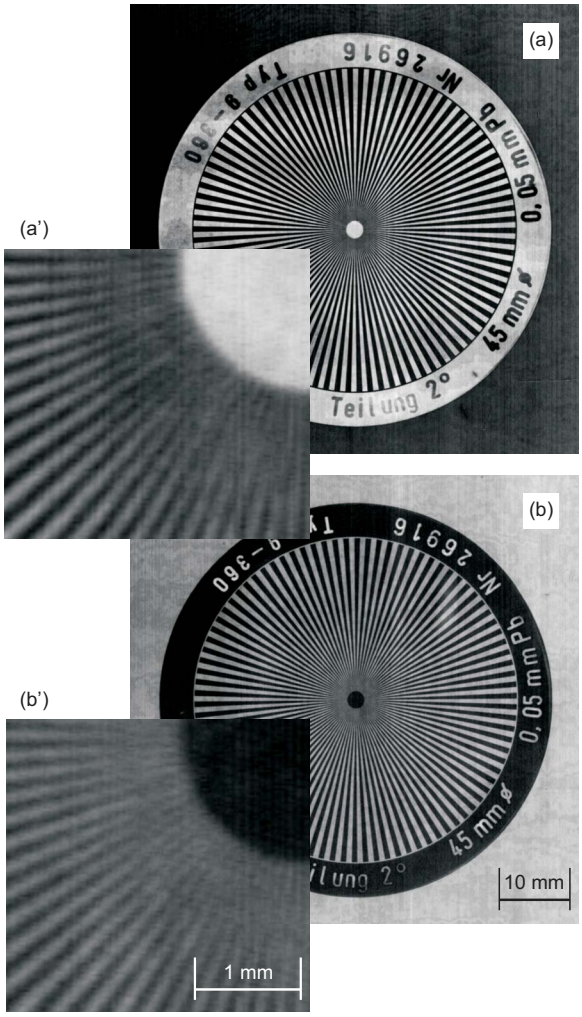

FIG. 9. Images of a 0.05-mm-thick lead star phantom acquired on our XLV prototype with (a) 0 V and (b) 40 V readout bias. The phantom is shown to scale, along with a 15 times magnification of the center in (a′) and (b′). The divisions are separated by 2° angles and the inner diameter of the ring is 45 mm. The grayscale values are reversed in both images due to a shift in the characteristic curve. The resolution limit visible in the magnified images is due to limitations in the optical components of the optical scanner.

(a′) and Fig. 9(b′), that there is no resolution difference related to this change in V_R. In both cases, the resolution limit is ~10 lp/mm.

Our prototype as shown in Fig. 5 establishes a proof of concept of the XLV. For clinical chest radiography purposes, key characteristics will be optimized: the thickness of the photoconductor will be increased to 1 mm, structural defects will be reduced through both improved construction methods and post-processing image correction, and the aluminum substrate used to hold the photoconductor will be thinned or completely replaced by a lower atomic number material. Furthermore, it is important to note that if the XLV has sufficient exposure latitude and spatial resolution requirements for chest radiography, it would also have sufficient exposure latitude for abdominal and musculoskeletal radiography.

VII. CONCLUSIONS

The electro-optical characteristics of a LC cell and the thickness of a photoconductor layer determine the optical properties of an XLV as a function of x-ray exposure. In order to be suitable for chest radiography, the LC cell must enable an XLV-based system to satisfy established imaging requirements. We identified and theoretically evaluated three simple reflective cell designs commonly used in display technology. The modeling results indicate that the r-ECB cell is the only cell which spans an imaging range wide enough to fulfill the requirements for chest radiography, provided that the characteristic curve can be shifted to lower exposures. Experimental measurements proved these shifts to be feasible. By applying an appropriate amount of readout bias potential during the digitization step, we adjusted the characteristic curve of our XLV prototype, consisting of an r-ECB cell design, to overcome the threshold voltage and the multi-valued optical response of the cell. By utilizing an r-ECB cell in connection with a 1-mm-thick photoconductive *a*-Se layer, we have shown that an XLV-based system has the potential to satisfy all requirements for digital chest radiography.

ACKNOWLEDGMENTS

We would like to thank Peter Oakham, Steven Germann, and Giovanni DeCrescenzo for useful discussions. We gratefully acknowledge financial support from the National Institutes of Health Grant No. 5-R01-EB-002-352-02 entitled "Low cost digital x-ray detectors using liquid crystals."

[a]Author to whom correspondence should be addressed; Electronic mail: john.rowlands@sri.utoronto.ca

[1]J. A. Rowlands and I. Yorkston, "Flat panel detectors for digital radiography," in *Handbook of Medical Imaging*, edited by J. Beutel, H. L. Kundel, and R. L. Van Metter (SPIE, Bellingham, 2000), pp. 223–328.
[2]P. Rieppo, B. Bahadur, and J. A. Rowlands, "Amorphous selenium liquid crystal light valve for x-ray imaging," in *Physics of Medical Imaging*, edited by R. L. Van Metter and J. Beutel, Proc. SPIE **2432**, 228–236 (1995).
[3]P. Rieppo and J. A. Rowlands, "X-ray imaging with amorphous selenium: Theoretical feasibility of the liquid crystal light value for radiography," Med. Phys. **24**, 1279–1291 (1997).
[4]C. A. Webster, I. Koprinarov, S. Germann, and J. A. Rowlands, "The x-ray light valve: A low-cost, digital radiographic imaging system—concept and implementation," Med. Phys. **35**, 939–949 (2008).
[5]J. A. Rowlands, C. A. Webster, I. Koprinarov, P. Oakham, K. C. Schad, T. Szeto, and S. Germann, "Low cost digital radiographic imaging systems: The x-ray light valve," in *Physics of Medical Imaging*, edited by M. J. Flynn and J. Hsiech, Proc. SPIE **6142**, 1–9 (2006).
[6]M. J. Foley, P. W. Walton, and W. J. van der Putten, "Development of an image receptor for use in digital mammography," in *Optics and Photonics Technologies and Applications*, edited by T. J. Glynn, Proc. SPIE **4876**, 54–61 (2003).
[7]W. Zhao and J. A. Rowlands, "X-ray imaging using amorphous selenium: Feasibility of a flat panel self-scanned detector for digital radiology," Med. Phys. **22**, 1595–1604 (1995).
[8]G. S. Belev, B. Fogal, K. V. Koughia, R. E. Johanson, and S. O. Kasap, "Dependence of charge carrier ranges in stabilized *a*-Se on preparation conditions and alloying," J. Mater. Sci.: Mater. Electron. **14**, 841–843 (2003).
[9]W. Que and J. A. Rowlands, "X-ray photogeneration in amorphous selenium: Geminate versus columnar recombination," Phys. Rev. B **51**, 10500–10507 (1995).
[10]P. Yeh and C. Gu, *Optics of Liquid Crystal Displays* (Wiley, New York, 1999).
[11]S. T. Wu and D. K. Yang, *Reflective Liquid Crystal Displays*, SID Series in Display Technology (Wiley, New York, 2005).
[12]C. H. Gooch and H. A. Tarry, "The optical properties of twisted nematic

liquid crystal structures with twist angles ⩽90°," J. Phys. D **8**, 1575–1584 (1975).
[13]T. Sonehara and O. Okumura, "A new twisted nematic ECB (TN-ECB) mode for a reflective light valve," in *Japan Display*, Proc. SPIE **31**, 192–195 (1989).
[14]H. S. Kwok, "Parameter space representation of liquid crystal display operating modes," J. Appl. Phys. **80**(7), 3687–3693 (1996).
[15]H. Fieldler and F. Laugwitz, "Zur quantenausbeute elektroradiograpischer selenschichten," J. Signal AM **9**, 229–235 (1981).
[16]J. A. Rowlands, G. DeCrescenzo, and N. Araj, "X-ray imaging using amorphous selenium: Determination of x-ray sensitivity by pulse height spectroscopy," Med. Phys. **19**, 1065–1069 (1992).
[17]K. C. Schad, I. Koprinarov, C. A. Webster, and J. A. Rowlands, "The x-ray light valve—prediction of the x-ray characteristic curve and its application to liquid-crystal-cell design," Med. Phys. (to be published).
[18]GNU-LCM was developed by Salman Saeed, BOSLab Research Group, Liquid Crystal Institute, Kent State University, Kent, OH, under funding from NATO. It uses the Birefringent Thin Films Toolbox developed and copyrighted by I. J. Hodgkinson and Q. Wu of the University of Otago, Dunedin, Otago, New Zealand.
[19]D. W. Berreman, "Optics in stratified and anisotropic media: 4×4-matrix formulation," J. Opt. Soc. Am. **62**(4), 502–510 (1972).
[20]*Liquid Crystal Mixtures For Electro-Optical Displays* (Merck Ltd./BDH Publication, 1992).
[21]D. M. Tucker, G. T. Barnes, and D. P. Chakraborty, "A semiempirical model for generating tungsten target x-ray spectra," Med. Phys. **18**, 211–218 (1991).
[22]D. L. Lee, L. K. Cheung, and L. S. Jeromin, "A new digital detector for projection radiography," Proc. SPIE **2432**, 237–249 (1995).